Original Article

Institution of MECHANICAL ENGINEERS
Journal of AEROSPACE ENGINEERING

Proc IMechE Part G:
J Aerospace Engineering
2018, Vol. 232(8) 1571–1583

DOI: 10.1177/0954410017696110
journals.sagepub.com/home/pig
SAGE

Pigeon-inspired optimization and lateral inhibition for image matching of autonomous aerial refueling

Yongbin Sun and Haibin Duan

Abstract

Autonomous aerial refueling (AAR) is an essential application of unmanned aerial vehicles for both military and civilian domains. In this paper, a hybrid algorithm of the pigeon-inspired optimization (PIO) and lateral inhibition (LI), called LI-PIO, is proposed for image matching problem of AAR. LI is adopted for image pre-processing to enhance the edges and contrast of images. PIO, inspired from the homing characteristics of pigeons, is a novel bio-inspired swarm intelligence algorithm. To demonstrate the effectiveness and feasibility of our proposed algorithm, we make extensive comparative experiments with particle swarm optimization (PSO), particle swarm optimization based on lateral inhibition (LI-PSO), and PIO. It can be concluded from the experimental results that our proposed LI-PIO has excellent performances for image matching problem of AAR, especially in convergent rate and computation speed.

Keywords

Pigeon-inspired optimization, lateral inhibition, unmanned aerial vehicles, autonomous aerial refueling, image matching

Date received: 13 April 2016; accepted: 1 February 2017

Introduction

Aerial refueling[1,2] is an effective method of increasing the endurance and range of aircrafts. In recent decades, with the progress of unmanned aerial vehicles (UAVs), aerial refueling has been developed to autonomous aerial refueling (AAR).[2,3] The realization of automation makes vision sensors and image processing essential. Visual system can play an important part in the visual guidance, measurement, and detection.[4–9] In the process of flying boom AAR, the tanker aircraft has to recognize the boom and receptacle accurately. The requirements can be satisfied by the image matching (template matching) method,[10] which is a process of searching the right sub-image in the reference image according to the known template.

The classical template matching method is based on gray cross-correlation measurement by comparing the template with the captured image pixel by pixel. In recent years, plenty of image matching methods have been developed[11–14] and they can be classified as the statistic-based algorithm and the feature-based algorithm.[10] The statistic-based algorithm analyzes the attributes of image that reflect the similarity between the template and the original image such as absolute difference, mean absolute difference, square difference, and mean square difference. The feature-based algorithm is based on the image features, such as border, unique points, texture, entropy, and energy. Compared with the statistic-based algorithm, the feature-based algorithm depends more on the circumstances. The statistic-based algorithm has stronger ability to suppress noise. Besides, it is easy to program and implement on hardware. Our proposed pigeon-inspired optimization based on lateral inhibition (LI-PIO) is one of the statistic-based algorithms.

In the matching process, all the possible positions in the original image have to be computed. Therefore, an effective algorithm is needed to shorten the tremendous time cost of matching. Among all the algorithms, swarm intelligence optimization algorithms have outstanding advantages in terms of accuracy and efficiency. Thus, in recent years, many global swarm intelligence optimization algorithms appear, including genetic algorithm (GA),[15] particle swarm

Science and Technology on Aircraft Control Laboratory, School of Automation Science and Electrical Engineering, Beihang University (BUAA), Beijing, PR China

Corresponding author:
Haibin Duan, Science and Technology on Aircraft Control Laboratory, School of Automation Science and Electrical Engineering, Beihang University (BUAA), No. 37, Xueyuan Road, Haidian District, Beijing 100191, PR China.
Email: hbduan@buaa.edu.cn

optimization (PSO),[16] artificial bee colony (ABC),[17] ant colony optimization (ACO),[18] biogeography-based optimization (BBO),[19] and brain storm optimization (BSO).[20] These swarm intelligence optimization algorithms have already been applied to image matching, air robot path planning, object segmentation, and other practical aspects. In this paper, our proposed LI-PIO is used for image matching and has good performances in terms of convergence speed, robustness, and stability.

Inspired by the homing characteristics of pigeons, Duan firstly proposed a novel swarm intelligence algorithm, pigeon-inspired optimization (PIO).[21] The basic PIO includes two operators: map and compass operator, and landmark operator. The two operators have different computational rules, which can adjust to different problems. In Duan's researches,[21] the PIO algorithm has proven itself feasible and effective for path planning. When the algorithm is applied to image matching, the superiority should appear as well. In this paper, we combine the PIO algorithm and lateral inhibition for image matching problem of AAR.

The remainder of this paper is organized as follows. The AAR system is presented in the forthcoming section. Next, the details of the PIO algorithm are introduced. Besides, the lateral inhibition mechanism is described in a later section. In subsequent sections, the hybrid of PIO and lateral inhibition including the detailed implementation procedures is specified and comparative experiments are given to demonstrate the effectiveness of LI-PIO. Conclusions are contained in the final section.

The autonomous aerial refueling system

The model of the AAR system

Three approaches are currently adopted for aerial refueling: the flying boom method, where the tanker extends the retractable boom to the fuel receptacle of receiver aircraft; the probe and drogue method, where the tanker drags a flexible hose with a drogue and the receiver aircraft aims at inserting the probe into the drogue; the boom drogue adapter units method, which is the combination of the above two methods by attaching the drogue adapter units to the boom. We mainly focus on the flying boom method in this paper.

The model of the AAR system in the experimental environment consists of tanker aircraft, receiver UAV, the boom, and visual system as shown in Figure 1. In our research, an octocopter and a quadcopter are adopted as the tanker aircraft and receiver UAV, respectively. A retractable boom, which can move in three degrees of freedom, is attached to the tanker. Besides, the onboard cameras are mounted on the tanker aircraft to capture the red cooperative markers around the receptacle of receiver UAV, which are used for the visual measurement.

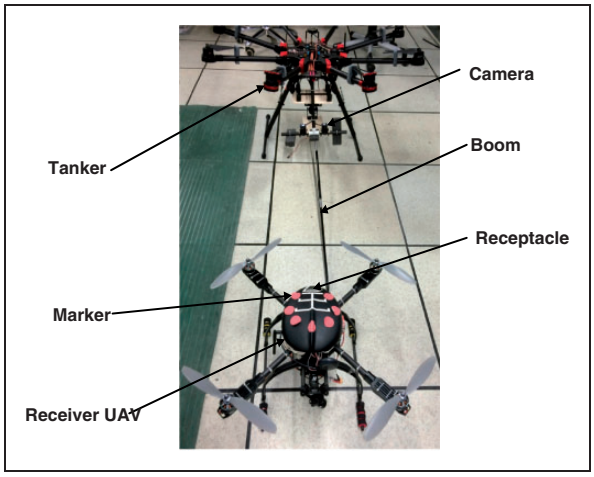

Figure 1. The model of the AAR system. UAV: unmanned aerial vehicle.

Figure 2. The formation flight.

The implementation of AAR system

AAR is a complex and difficult problem in the global world. To some extent, the procedure of AAR is similar to the formation flight[22,23] as shown in Figure 2. The tanker aircraft and the receiver UAV have to cooperate with each other. The controllers of tanker aircraft and receiver UAV need to know the pose, speed, and position information of the two aircrafts.

As shown in Figure 3, there are four important procedures: data fusion, visual measurement, boom control, and station-keeping control. The data of global positioning system (GPS)[24,25] and inertial navigation system (INS) are fused to locate the positions of aircrafts. However, the accurate poses of receptacle cannot be supplied or estimated by GPS and INS. Thus, binocular vision measurement is used to estimate the accurate poses. Besides, the boom control system is obbligato to complete the docking of AAR. In order to realize the optimal nonlinear control, it is necessary to develop the model of atmospheric turbulence and flying boom. The dynamic model of flying boom can be developed using the

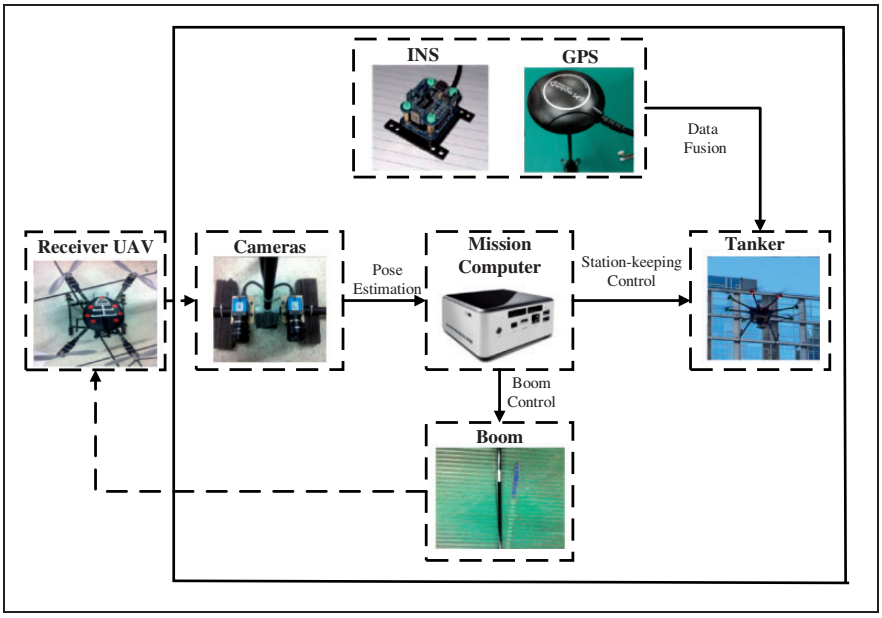

Figure 3. The framework of AAR system.
UAV: unmanned aerial vehicle; INS: inertial navigation system; GPS: global positioning system.

state-space approach. And the atmospheric turbulence can be modeled as the Dryden model. Moreover, once images are captured by the cameras, the mission computer would implement marker detection, point matching, and pose estimation during the docking. Marker detection is the premise of visual measurement. And the detected markers must be transformed from the camera coordinate to the aircraft coordinate. Point matching is required to associate the prior coordinates with the makers. Furthermore, during the docking of AAR, the tanker aircraft and receiver UAV have to keep an appropriate position relation to avoid collision and separation. A proportional guidance law with feedforward of velocities is designed to realize the station-keeping control for AAR.

In the procedure of visual measurement, our proposed LI-PIO method can accurately extract features for image matching, which plays an important part in AAR.

The pigeon-inspired optimization algorithm

Pigeon is a popular kind of bird in the world. In ancient China, pigeons were regarded as an important communication tool, which can be applied not only to the daily life, but also to the military situations. During the First and Second World War, pigeons played a critical role in seeding military intelligence due to their concealment and veracity. Thus, extensive research has been carried out on pigeons where it was discovered that pigeons can easily find their destinations by using three methods: magnetic field, sun, and landmarks. Inspired by the homing pigeons, Duan and Qiao[21,26] firstly put forward the PIO algorithm, which has been applied to the path planning of air robot and target detection.

The basic PIO includes two operators: map and compass operator and landmark operator.[21]

The map and compass operator model is based on the magnetic field and sun, while the landmark operator model is based on landmarks. Therefore, the process of basic PIO is as follows.[21]

Map and compass operator. When the evolutionary iteration is less than the operator's maximum, the algorithm relies on the map and compass operator as shown in Figure 4, which means the pigeons are far from the destination. Each pigeon has a position and a velocity of evolution. Suppose the position and the velocity of pigeon i are X_i, V_i. For a n-dimension search space, $X_i = [x_i^1, x_i^2, \ldots, x_i^n]$, $V_i = [v_i^1, v_i^2, \ldots, v_i^n]$; in this paper, it is a two-dimensional search problem for image matching corresponding to the pixel's position (m, n). The new position X_i and velocity V_i of pigeon i at the tth iteration are updated as follows[21]

$$V_i(t) = V_i(t-1) \cdot e^{-Rt} + rand \cdot \left(X_g - X_i(t-1)\right) \tag{1}$$

$$X_i(t) = X_i(t-1) + V_i(t-1) \tag{2}$$

where R is the map and compass factor, which makes the velocity of evolution slow down as the iteration goes. $rand$ is a rand number within $[0, 1]$. X_g is the global best position, which indicates the maximum fitness value among all pigeons.

Landmark operator. In landmark operator, as shown in Figure 5, pigeons would fly straight to their destination if they are familiar with the landmarks. With respect to the pigeons still far from the destination, they are unfamiliar with the landmarks.

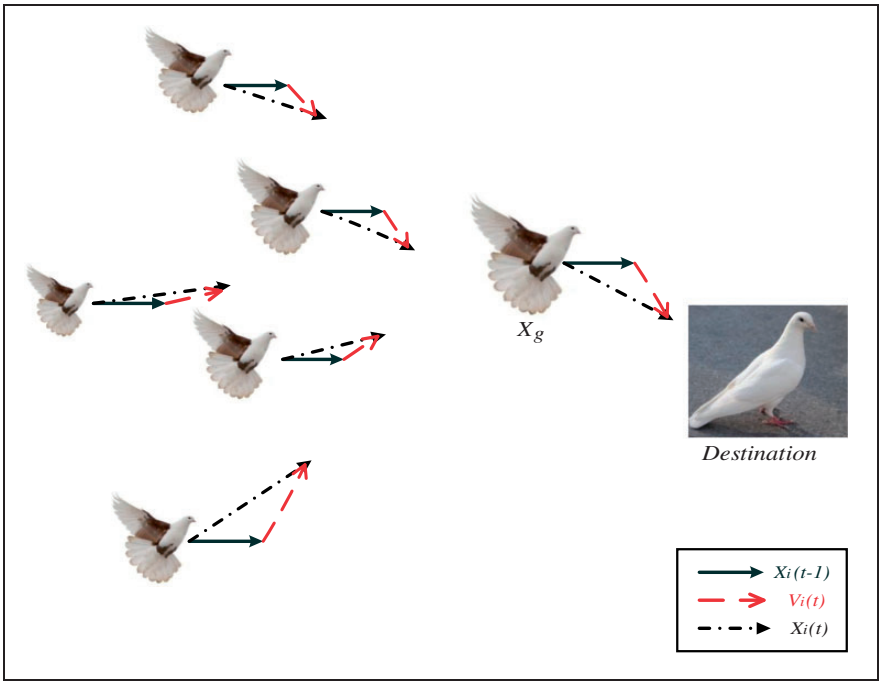

Figure 4. The process of map and compass operator evolution.

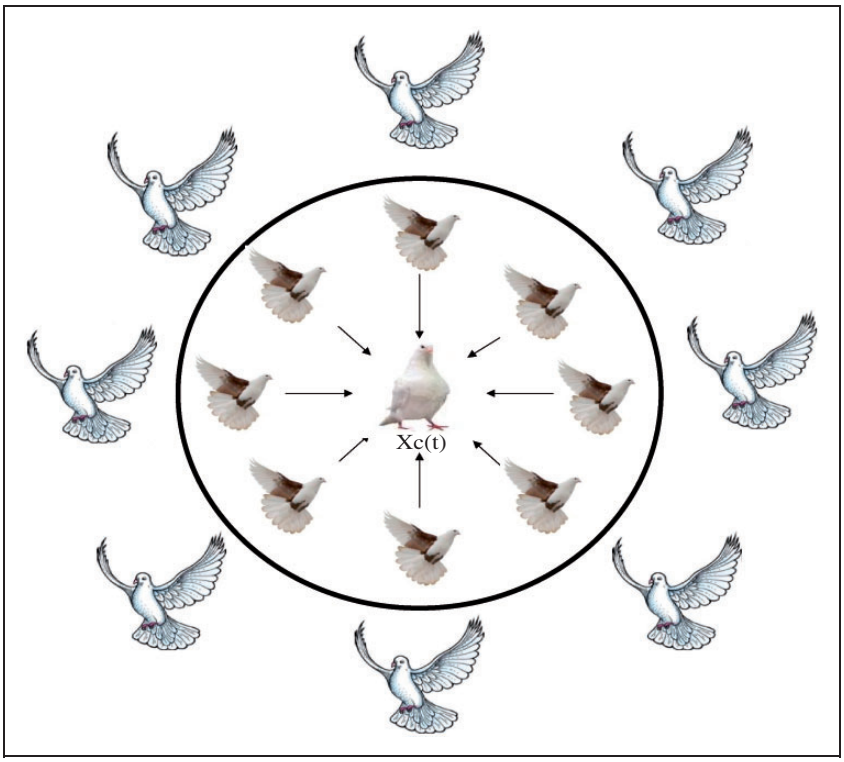

Figure 5. The process of landmark operator evolution.

These pigeons far from the destination (pigeons outside the big black circle in Figure 5) would follow those that are familiar with the landmarks. In landmark operator, half of the pigeons would regard the center of the pigeons as their destination and they would fly straight to the center, as the pigeons in the big black circle in Figure 5. Thus, the number of pigeons would be decreased by half in every iteration. Let $X_c(t)$ be the center of some pigeons at the tth iteration, the position of pigeon i at the tth iteration can be calculated by the following equations[14]

$$N_p(t) = \frac{N_p(t-1)}{2} \tag{3}$$

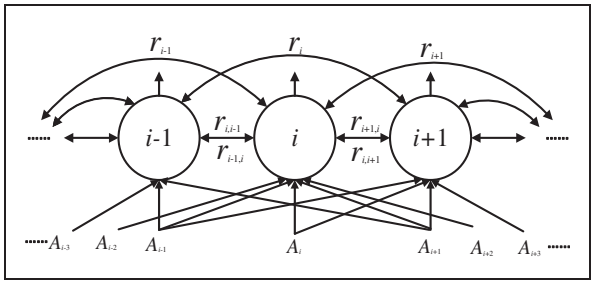

Figure 6. The lateral inhibition in neural system.

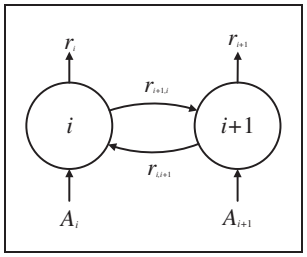

Figure 7. The lateral inhibition between two units.

$$X_c(t) = \frac{\sum_{Np} X_i(t) \cdot fitness(X_i(t))}{\sum fitness(X_i(t))} \tag{4}$$

$$X_i(t) = X_i(t-1) + rand \cdot \left(X_c(t) - X_i(t-1)\right) \tag{5}$$

where *fitness*() is the fitness function, which can determine the quality of each pigeon.

The lateral inhibition mechanism

Lateral inhibition is a phenomenon, which a neuron in the neural system that inhibits its neighbors to compete with the other neurons. This phenomenon exists in the visual cortex as well as auditory cortex. Though lateral inhibition was realized for a long time, the mechanism was not used to practical application. Since Hartline[27] and his research team carried out an electrophysiology experiment on the eyes of limulus, the mechanism started to be applied to a lot of fields, especially in the visual field.

Lateral inhibition has a great importance in the pre-processing of images because of its effect on the enhancement of the image's edges or contours between the regions of different intensities. Moreover, the image matching is based on the difference of images. The more the gray levels in an image, the more the noise levels in an image. Thus, in this paper, we diminish the gray levels to two levels, which can filter the image to decrease the noise. Besides, by diminishing the gray levels, the computational complexity can be decreased. In this way, when matching all the possible positions in the original image, the time cost will be decreased.

Neurons in the neural system are connected and are as shown in Figure 6.[28] There are overlaps of receptive fields at input as well as at output. One neuron's output not only depends on its inputs, but on its neighbors' inputs and outputs. In terms of lateral inhibition, the nearer the neurons, the larger will be the inhibition of neurons. In addition, the inhibition of two neurons is approximately linear.[27]

Hartline[27] in his work took care of two microphthalmias of limulus' eyes separately similar to the two neurons in the neural system, as shown in Figure 7. In the retinal image, the excited receptors in illuminated light areas inhibit those in dark areas more strongly than the latter to the former. Thus, the construct and the distortion of sensory information are enhanced.

Supposing the excitatory stimuli of different frequencies are input to the two mircophthalmias as shown in Figure 7, the outputs are presented as the following due to the lateral inhibition's linear property[27]

$$\begin{cases} r_i = e_i - k_{i,i+1}(r_{i+1} - r^0_{i,i+1}) \\ r_{i+1} = e_{i+1} - k_{i+1,i}(r_i - r^0_{i+1,i}) \end{cases} \tag{6}$$

where r_i, r_{i+1} are the outputs of two units considering the function of lateral inhibition. A_i, A_{i+1} are the separate inputs of the two units. $k_{i,i+1}$, $k_{i+1,i}$ are the linear coefficients of lateral inhibition, $k_{i,i+1}(r_{i+1} - r^0_{i,i+1})$ equals $r_{i,i+1}$ in Figure 7 as well as $r_{i+1,i}$. $r^0_{i,i+1}$, $r^0_{i+1,i}$ are the threshold values of linear lateral inhibition.

When all the microphthalmias (units) were taken into account, Hartline and his colleagues put forward the following classical lateral inhibition model

$$\begin{aligned} r_p &= e_p - \sum_{j=1}^{n} k_{pj}(r_j - r^0_{pj}) \quad p = 1, 2, \ldots, n\,; \\ & j = 1, 2, \ldots, n\,; j \neq p \end{aligned} \tag{7}$$

where e_p is the output of unit without lateral inhibition; k_{pj} denotes the linear coefficients; r_p, r_j represent the outputs of two units; r^0_{pj} is the threshold value.

In order to apply this mechanism to image processing, equation (7) is transformed to a two-dimensional and gray form. Through the effect of lateral inhibition, the output gray $P(m,n)$ is given as follows[29]

$$\begin{aligned} P(m,n) &= f\left[\sum_{i=-M}^{M}\sum_{j=-N}^{N} \alpha_{i,j} I_0(m+i, n+j)\right] \\ &= f[R_0(m,n)] \end{aligned} \tag{8}$$

where $\alpha_{i,j}$ is the lateral inhibition coefficient of *pixel*(*m*,*n*) to the central pixel. $I_0(m,n)$ is the original gray value of *pixel*(*m*,*n*). $P(m,n)$ is the gray value of *pixel*(*m*,*n*) processed by lateral inhibition.

$R_0(m,n)$ denotes the lateral inhibition competing coefficient of the *pixel*(*m*,*n*). f represents the inhibition competing relation function between the output and input. $(2M+1)\times(2N+1)$ is the receptive field.

In the vision nerve system, one nerve cell is fairly stable and consistent with its surrounding nerve cells. The input image is not constrained to directions. Thus, the weight values are mutually symmetric according to the center. The size of the receptive field can be 3×3, 5×5, 7×7 and we choose 5×5 in this paper. Then, the competing coefficient of the lateral inhibition network is as follows

$$\begin{aligned} R_0(m,n) = {} & \alpha_{00}\times I_0(m,n) \\ & + \alpha_1\left[\sum_{i=-1}^{1}\sum_{j=-1}^{1} I_0(m+i,n+j) - I_0(m,n)\right] \\ & + \alpha_2\left[\sum_{i=-2}^{2}\sum_{j=-2}^{2} I_0(m+i,n+j)\right. \\ & \left. - \sum_{i=-1}^{1}\sum_{j=-1}^{1} I_0(m+i,n+j)\right] \end{aligned} \tag{9}$$

where α_{00} denotes the weight value of the center, α_1 is the surrounding weight value of the center, and α_2 represents the peripheral weight value.

And the lateral inhibition coefficient satisfies

$$\alpha_{00} + 8\alpha_1 + 16\alpha_2 = 0 \tag{10}$$

In this paper, we choose $\alpha_{00}=1$, $\alpha_1=-0.075$, and $\alpha_2=-0.025$. Then, equation (9) can be described as follows

$$R_0(m,n) = I_0(m,n)\otimes Q \tag{11}$$

$$Q = \begin{bmatrix} -0.025 & -0.025 & -0.025 & -0.025 & -0.025 \\ -0.025 & -0.075 & -0.075 & -0.075 & -0.025 \\ -0.025 & -0.075 & 1 & -0.075 & -0.025 \\ -0.025 & -0.075 & -0.075 & -0.075 & -0.025 \\ -0.025 & -0.025 & -0.025 & -0.025 & -0.025 \end{bmatrix} \tag{12}$$

where $\otimes$ denotes the convolution operation, Q represents the lateral inhibition matrix of 5×5 receptive field.

After combining the modulus template Q with equation (9), a new gray scale of the image can be obtained, which is $R_0(m,n)$. Finally, the image's edges are extracted by the following equation

$$P(m,n) = \begin{cases} 255 \ldots\ldots\ldots R_0(m,n) \geqslant T \\ 0 \ldots\ldots\ldots\ldots R_0(m,n) < T \end{cases} \tag{13}$$

where T is a user-defined threshold value, which is different in different practical situations. $P(m,n)$ is the gray value of the original gray value *pixel*(*m*,*n*) processed by the lateral inhibition.

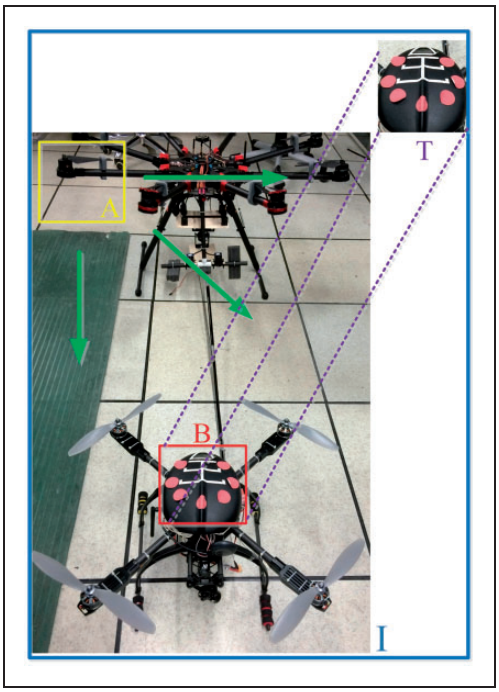

Figure 8. Illustration of LI-PIO for image matching. The template image *T* is in the top right corner; the yellow box *A* denotes the search box, which searches along the green arrow in the full image *I* by LI-PIO algorithm; finally, the best matching result would be obtained inside the red box *B*.

Table 1. The image matching method, fitness() function.

```
Begin
  fitness = 0;
  for i = 0:M − 1
    for j = 0:N − 1
      if P(x0 + i, y0 + j) = Pt(i, j) then
        fitness = fitness + 1;
      end if
    end for
  end for
End
```

Table 2. The parameters of LI-PIO algorithm.

Parameter	Description	Value
n	Number of pigeons	200
NC_{max}	Maximum times of iteration	150
$NC1_{max}$	The iteration of map and compass operator	100
$NC2_{max}$	The iteration of landmark operator	50
R	The map and compass factor	0.2
D	Dimensions of the search problem	2
T	The threshold of lateral inhibition	115

Hybrid PIO and lateral inhibition

The fitness function of LI-PIO

In order to evaluate the quality of each pigeon (solution), the fitness function is often defined. Pigeon at the better position has the bigger fitness value. And pigeons with little fitness value fly to those with bigger fitness value. In addition, all the pigeons fly to the position that has the maximum fitness value. The larger the fitness value, better will be the template image matching. In this paper, the fitness function is chosen as follows, which is simple and easy to program.

$$fitness(t) = fitness(t-1) + 1 \tag{14}$$

As presented in Table 1, $M \times N$ is the size of the template image. $P(x_0, y_0)$ is the gray value of the original image. Suppose the size of original image is $A \times B$, the searching ranges of x_0 and y_0 are $0 \leqslant x_0 < A - M + 1$, $0 \leqslant y_0 < B - N + 1$. $P(x_0 + i, y_0 + j)$ is the gray value of the pixel in the original image.

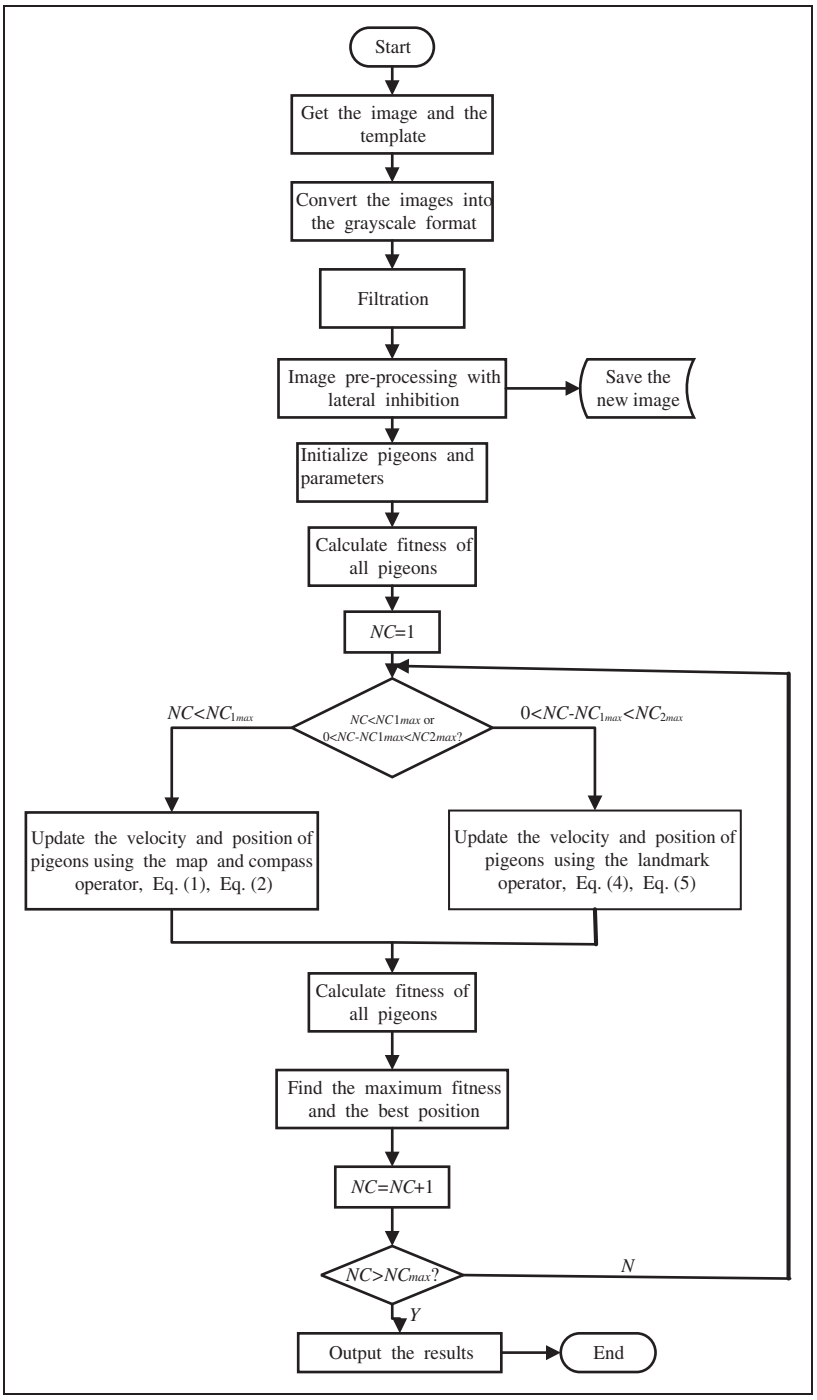

Figure 9. Detailed flow chart of LI-PIO for image matching.

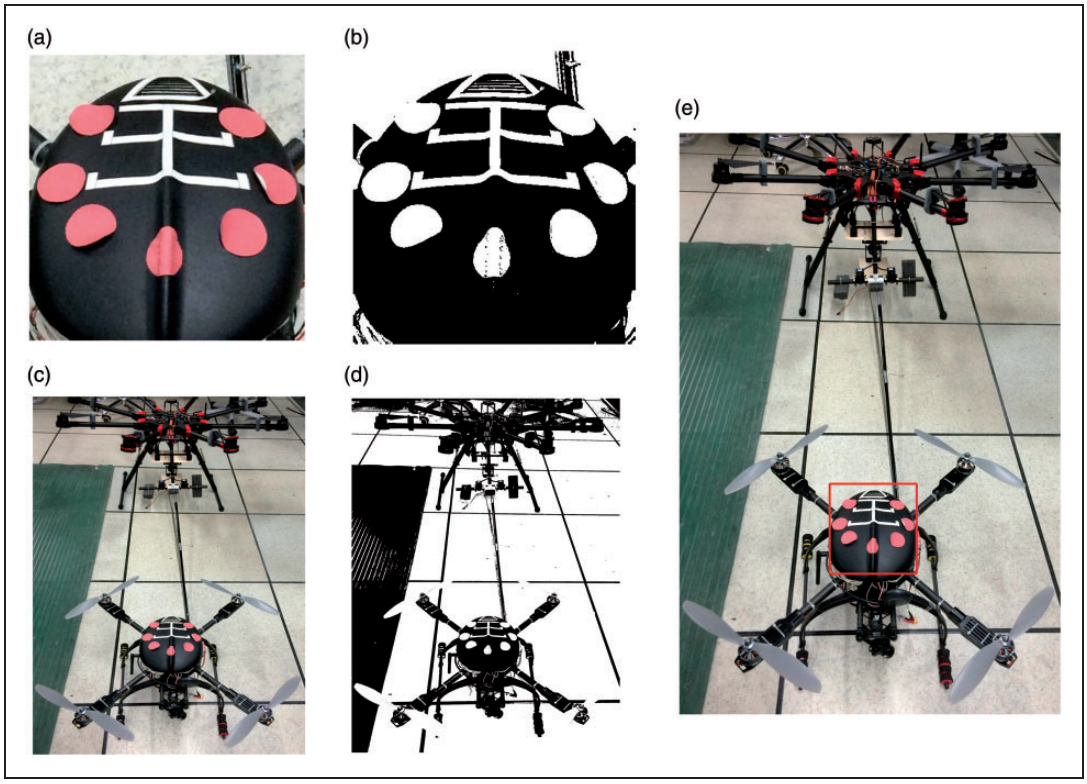

Figure 10. Matching results for case 1: (a) template image (451×436); (b) template image processed by lateral inhibition; (c) original image (2901×1901); (d) original image processed by lateral inhibition; (e) matching result by LI-PIO.

$P_t(i,j)$ is the gray value of the pixel in the template, $0 \leqslant i \leqslant M-1$, $0 \leqslant j \leqslant N-1$. In one loop, if $P(x_0+i, y_0+j) = P_t(i,j)$ is satisfied, the fitness value is calculated by equation (14).

The procedure of the LI-PIO for image matching

LI-PIO combines the PIO algorithm and lateral inhibition to solve the template matching problem of AAR, as shown in Figure 8. Our proposed method has better properties with high accuracy and efficiency, compared with PSO, LI-PSO, PIO in the subsequent section.

The procedure of LI-PIO for image matching is described as follows.

Step 1: Image pre-processing.

Obtain the original image and the template image, and convert them into gray scale format. Filter images to remove the noise. Then set different thresholds for different situations in order to pre-process the images by lateral inhibition. And save the new matrices of the images.

Step 2: Initialization of the pigeons and parameters.

Initialize pigeon's positions, velocities, and the parameters of this algorithm as shown in Table 2.

Step 3: Calculate each pigeon's fitness value according to Table 1.

Step 4: Update the pigeons.

When $NC \leqslant NC1_{\max}$, update the pigeons using the map and compass operator. The velocity and position of each pigeon are computed by equations (1) and (2). When $0 < NC - NC1_{\max} \leqslant NC2_{\max}$, update the pigeons using the landmark operator. The velocity and position of each pigeon are computed by equations (3) to (5).

Step 5: Calculate each pigeon's fitness value according to Table 1. And find out the maximum fitness and the best position for the image matching.

Step 6: Terminate if the current number of iterations NC reaches the $NC_{\max}$, output the results. Otherwise, go to step 4.

The algorithm flow for image matching is shown in Figure 9.

Comparative experimental analysis

In this section, series of experiments are given to verify the feasibility and effectiveness of our proposed LI-PIO for image matching. Besides, the results of LI-PIO, PSO, LI-PSO, and PIO are implemented as contrastive experiments. The parameters of LI-PIO are presented in Table 2. And the basic parameters

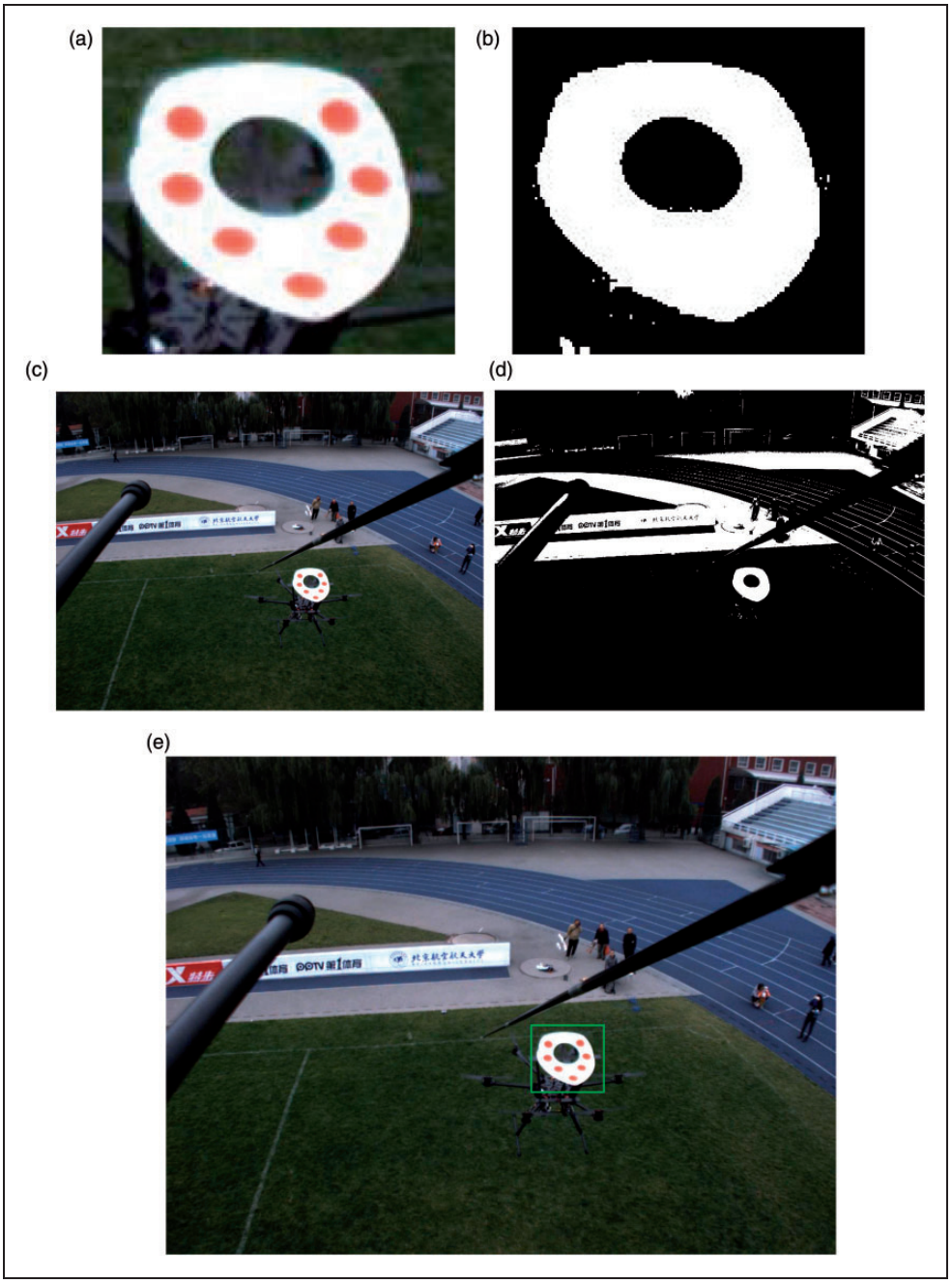

Figure 11. Matching results for case 2: (a) template image (131×141); (b) template image processed by lateral inhibition; (c) original image (964×1292); (d) original image processed by lateral inhibition; (e) matching result by LI-PIO.

of PSO, LI-PSO, and PIO are the same as those of LI-PIO. All the experiments are implemented in MATLAB 7.14.0(R2012a) on an i7 3.60 GHz computer with 4GB RAM.

For case 1, the results of LI-PIO are shown in Figure 10. The template image (451×436) and original image (2901×1901) are respectively shown in Figure 10(a) and (c). The template and original images processed by lateral inhibition are given in Figure 10(b) and (d). Eventually, we present the matching results obtained by LI-PIO in Figure 10(e). Another complex case is shown in Figure 11 to verify the function of the LI-PIO algorithm. The images of case 2 are acquired when we take outfield experiment, whose spatial resolution is a little lower to satisfy the requirement of the real timing.

Table 3. The contrast values of experimental images.

Images	Contrast values	Images	Contrast values
Figure 10(a)	0.0723	Figure 11(a)	0.2540
Figure 10(b)	0.1135	Figure 11(b)	0.4448
Figure 10(c)	0.0999	Figure 11(c)	0.1608
Figure 10(d)	0.1103	Figure 11(d)	0.3625

From the results shown in Figures 10 and 11, it is obvious that lateral inhibition enhances the edges of

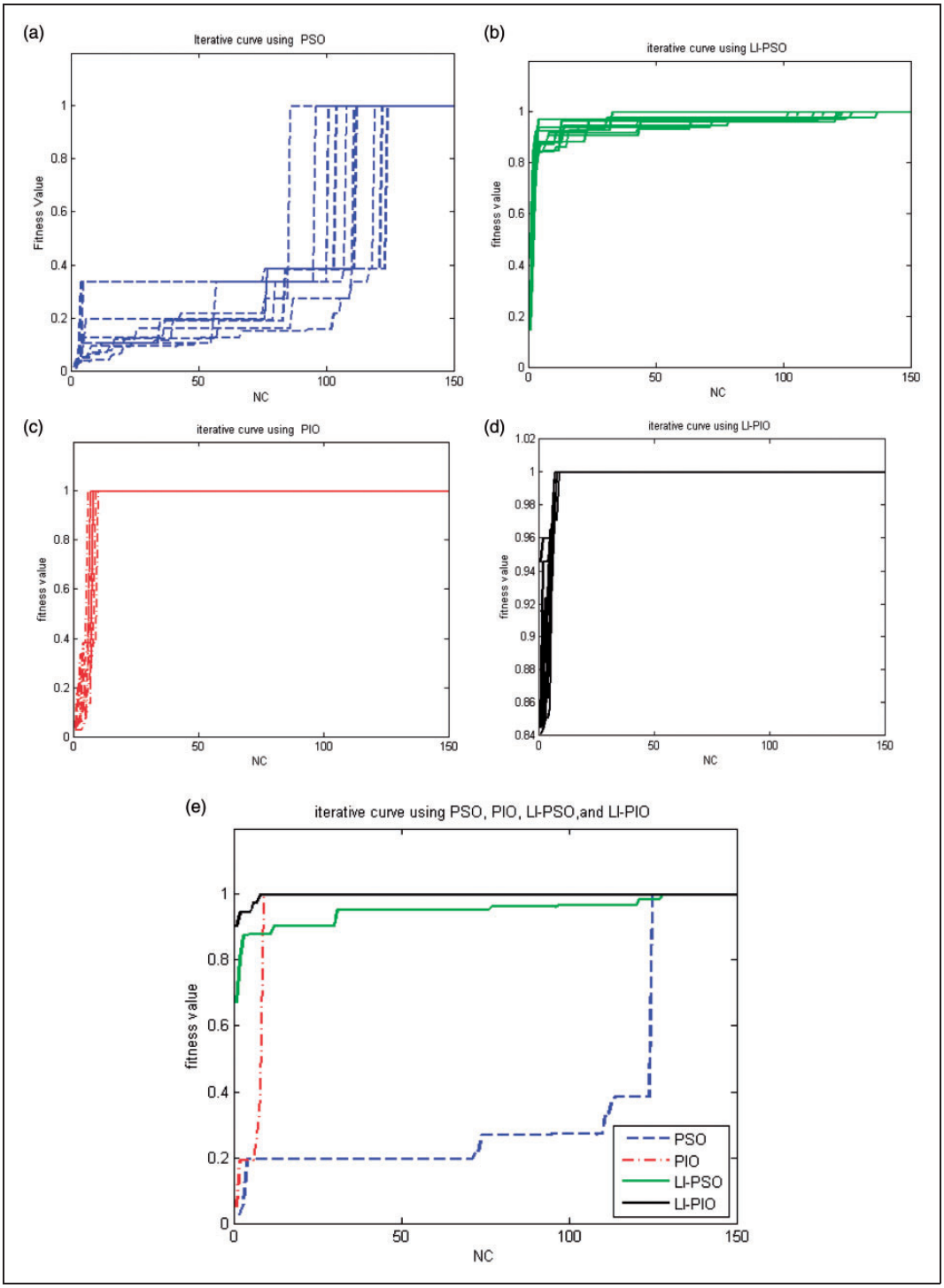

Figure 12. Comparative experiments for case 1: (a) independent 10 evolutionary curves of PSO; (b) independent 10 evolutionary curves of LI-PSO; (c) independent 10 evolutionary curves of PIO; (d) independent 10 evolutionary curves of LI-PIO; (e) evolutionary curves in comparison.
PSO: particle swarm optimization; PIO: pigeon-inspired optimization; LI: lateral inhibition.

Table 4. The average cost time of algorithms.

Algorithm	Cases	Time/s (150 iterations)
PSO	Case 1	716.0168
	Case 2	13.2352
LI-PSO	Case 1	1074.7
	Case 2	16.1668
PIO	Case 1	389.7384
	Case 2	5.9832
LI-PIO	Case 1	534.3799
	Case 2	8.2239

PSO: particle swarm optimization; PIO: pigeon-inspired optimization; LI: lateral inhibition.

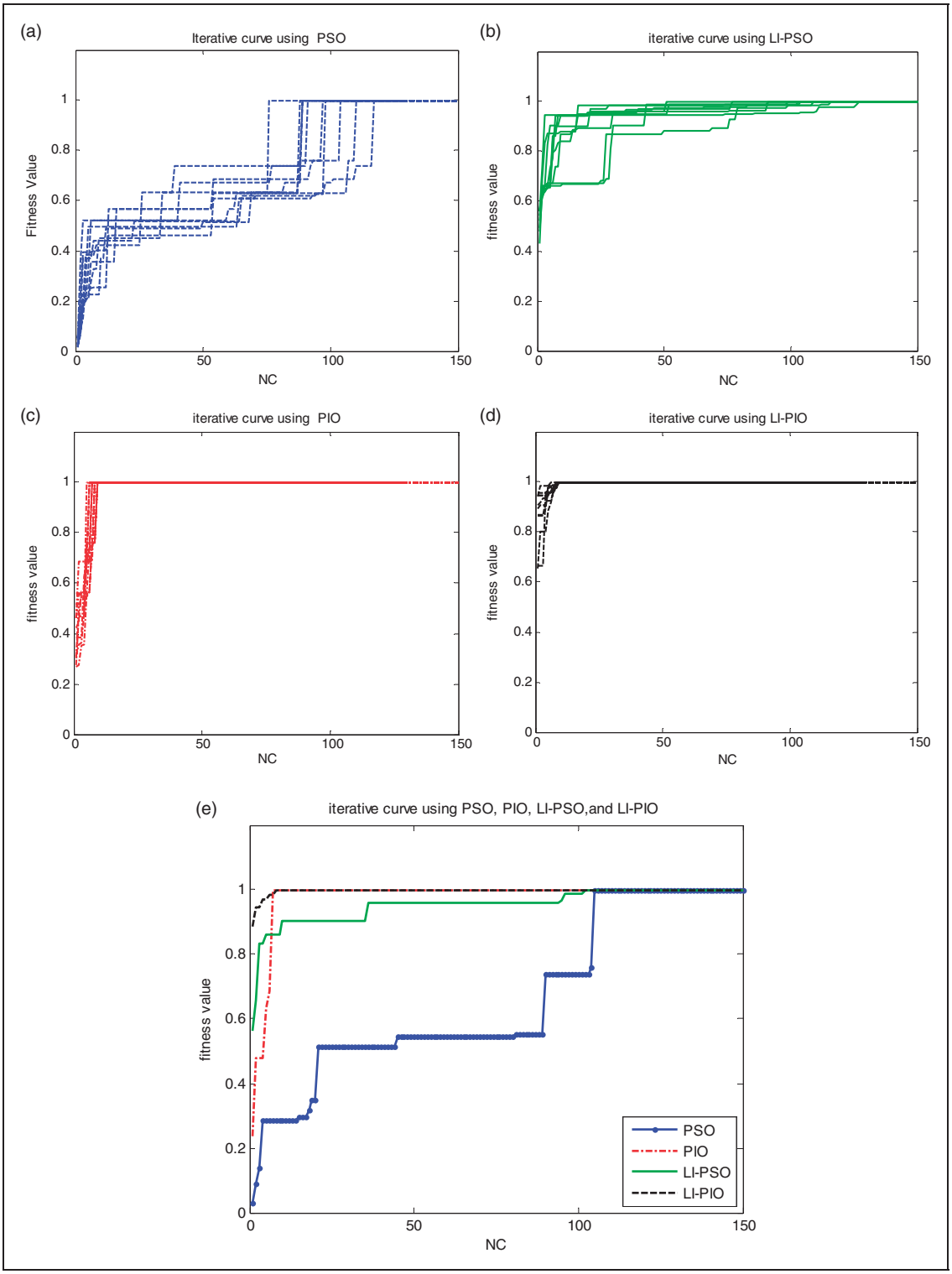

Figure 13. Comparative experiments for case 2: (a) independent 10 evolutionary curves of PSO; (b) independent 10 evolutionary curves of LI-PSO; (c) independent 10 evolutionary curves of PIO; (d) independent ten evolutionary curves of LI-PIO; (e) evolutionary curves in comparison.
PSO: particle swarm optimization; PIO: pigeon-inspired optimization; LI: lateral inhibition.

template and original images. Especially for case 2, the spatial resolution of the images is stressed to resolve the blurry problem. And the saliency of template image is improved as well. Supposing we calculate the ratio of image's standard deviation and average to present the contrast, the contrasts of the images are obviously enhanced as shown in Table 3. Due to the function of lateral inhibition, all the contrastive values increase extensively. Especially, the contrastive values of the template images improve by a large proportion, which is meaningful for obtaining the best matching result in the original image.

Besides, the value of Figure 11(d) is raised twice than in Figure 11(c), which reveals that the lateral inhibition is quite appropriate for the real experimental case. In addition, lateral inhibition filters the images to remove the noise.

To compare the feasibility and effectiveness, the evolutionary curves of PSO, LI-PSO, PIO, and LI-PIO are given in Figure 12. Furthermore, the cost time of all the algorithms are shown in Table 4, where the cost time is the average of 10 independent experiments.

In Figures 12 and 13, the evolutionary curves of PSO, LI-PSO, PIO, and LI-PIO are all presented. For contrastive purpose, the fitness values of different methods are normalized. It can be seen from Figures 12 and 13 that PSO acquires the best position and maximum fitness value at about the 100th iteration. Comparatively, the best position and maximum fitness value of PIO can be obtained at about 10th iteration. Moreover, owing to the function of lateral inhibition, LI-PSO and LI-PIO obtain larger fitness values from the beginning with the cost of a little time, which is conducive to promote the convergence of algorithms and find the best matching results. Furthermore, as presented in Table 4, LI-PIO can shorten about a half time per 150 iterations compared with LI-PSO for both the two cases. Therefore, it can be concluded that PIO converges much faster than PSO and the lateral inhibition mechanism plays an essential part in avoiding the local optimization to acquire the best fitness values. Thus, the combination of the LI and PIO balance the time costing and optimal matching results. For image matching problem of AAR, our proposed LI-PIO is reliable, feasible, and effective.

Conclusions

This paper presents a hybrid algorithm of the pigeon-inspired optimization and lateral inhibition for the image matching problem of AAR. PIO algorithm is a novel bio-inspired swarm intelligent algorithm, which can converge much faster than PSO. And the lateral inhibition mechanism is applied to enhance the edges and contrast of the images for pro-processing. The hybrid of PIO and LI inherits both advantages. The results of the comparative experiments indicate that our proposed LI-PIO method can not only obtain the optimal matching results but also shorten the time costing. Therefore, it can be concluded that LI-PIO is a more reliable, feasible, and effective image matching method with fast convergence rate. However, the effect of image matching depends a little on the threshold of LI, which means that improper thresholds lead to wrong results. But, the threshold can take an arbitrary value of a numerical range, which is easy to determine. Future work will focus on developing an adaptive algorithm to find the optimal thresholds of different experimental scenes. Besides, we will apply the LI-PIO algorithm to more complicated scenes in the complicated noisy environments. The LI-PIO algorithm will be an important bio-inspired swarm intelligent algorithm for image matching problem of AAR with extensive application prospects.

Declaration of Conflicting Interests

The author(s) declared no potential conflicts of interest with respect to the research, authorship, and/or publication of this article.

Funding

The author(s) disclosed receipt of the following financial support for the research, authorship, and/or publication of this article: This work was partially supported by the National Natural Science Foundation of China (Grant Nos. 61333004, 61273054, 61175109, and 61673327), and Aeronautical Foundation of China (Grant No. 20135851042).

References

1. Dell'Aquilla RV, Campa G, Napolitano MR, et al. Real-time machine-vision-based position sensing system for UAV aerial refueling. *J Real-Time Image Process* 2007; 1: 213–224.
2. Ding M, Wei L and Wang BF. Vision-based estimation of relative pose in autonomous aerial refueling. *Chinese J Aeronaut* 2011; 24: 807–815.
3. Thomas PR, Bhandari U, Bullock S, et al. Advances in air to air refueling. *Aerosp Sci* 2014; 71: 14–35.
4. Srinivasan MV, Zhang SW, Chahl JS, et al. An overview of insect-inspired guidance for application in ground and airborne platforms. *Proc IMechE, Part G: J Aerospace Engineering* 2004; 218: 375–388.
5. Lawson NJ. The application of laser measurement techniques to aerospace flows. *Proc IMechE, Part G: J Aerospace Engineering* 2004; 218: 33–57.
6. Lee D, Kim Y and Bang H. Vision-aided terrain referenced navigation for unmanned aerial vehicles using ground features. *Proc IMechE, Part G: J Aerospace Engineering* 2014; 228: 2399–2413.
7. Shah SIA, Wu AD and Johnson EN. A real-time simple light detection application for a flying robot in extreme noise and interference. *Proc IMechE, Part G: J Aerospace Engineering* 2014; 228: 2266–2285.
8. Shim SW, Won DY, Tahk MJ, et al. Vision-based long-range target detection using coarse-to-fine particle filter. *Proc IMechE, Part G: J Aerospace Engineering* 2014; 228: 1996–2006.
9. Li XL, Yang JH, Zhang L, et al. A new star pattern identification technique using an improved triangle algorithm. *Proc IMechE, Part G: J Aerospace Engineering* 2015; 229: 1730–1739.
10. Ma L, Sun Y, Feng N, et al. Image fast template matching algorithm based on projection and sequential similarity detecting. In: *Proceedings of the 5th international conference on intelligent information hiding and multimedia signal processing*, Kyoto, Japan, 2009, pp.957–960.
11. Koutaki G, Yata K, Uchimura K, et al. Fast and high accuracy pattern matching using multi-stage refining eigen template. In: *19th Korea-Japan joint workshop on*

frontiers of computer vision (FCV), Incheon, Korea (South), 2013, pp. 58–63.
12. Elboher E and Werman M. Asymmetric correlation: A noise robust similarity measure for template matching. *IEEE Trans Image Process* 2013; 99: 1–12.
13. Duan HB, Xu C, Liu S, et al. Template matching using chaotic imperialist competitive algorithm. *Pattern Recogn Lett* 2010; 31: 1868–1875.
14. Wang XH, Duan HB and Luo DL. Cauchy biogeography-based optimization based on lateral inhibition for image matching. *Optik* 2013; 124: 5447–5453.
15. Henry Holland J. *Adaptation in natural and artificial systems*. Ann Arbor, MI: University of Michigan Press, 1975.
16. Kennedy J and Eberhart R. Particle swarm optimization. In: *Proceedings of IEEE international conference on neural networks*, Perth, Australia, 1995, pp.1942–1948.
17. Sun CH and Duan HB. Artificial bee colony optimized controller for MAV pendulum. *Aircraft Eng Aerosp Technol* 2013; 85: 104–114.
18. Duan HB. *Ant colony algorithms: Theory and applications*. Beijing: Science Press, 2005.
19. Simon D. Biogeography-based optimization. *IEEE Trans Evolut Comput* 2008; 12: 702–713.
20. Duan HB and Li C. Quantum-behaved brain storm optimization approach to solving Loney's solenoid problem. *IEEE Trans Magnet* 2014; DOl: 10.1109/TMAG. 2014. 2325797.
21. Duan HB and Qiao PX. Pigeon-inspired Optimization: a new swarm intelligence optimizer for air robot planning. *Int J Intell Comput Cybernet* 2014; 7: 24–37.
22. Duan HB, Luo QN, Ma GJ, et al. Hybrid particle swarm optimization and genetic algorithm for multi-UAVs formation reconfiguration. *IEEE Comput Intell Magaz* 2013; 8: 16–27.
23. Duan HB and Liu SQ. Non-linear dual-mode receding horizon control for multiple unmanned air vehicles formation flight based on chaotic particle swarm optimization. *IET Control Theory Appl* 2010; 4: 2565–2578.
24. Fang JC and Gong XL. Predictive iterated Kalman filter for INS/GPS integration and its application to SAR motion compensation. *IEEE Trans Instrum Meas* 2010; 59: 909–915.
25. Sheimy NE, Chiang KW and Noureldin A. The utilization of artificial neural networks for multisensor system integration in navigation and positioning instruments. *IEEE Trans Instrum Meas* 2010; 59: 470–479.
26. Li C and Duan HB. Target detection approach for UAVs via improved pigeon-inspired optimization and edge potential function. *Aerosp Sci Technol* 2014; 39: 352–360.
27. Hartline HK. The response of single optic nerve fibers of the vertebrate eye to illumination of the retina. *Am J Physiol* 1938; 121: 400–415.
28. Arkachar P and Wagh MD. Criticality of lateral inhibition for edge enhancement in neural systems. *Neurocomputing* 2007; 70: 991–999.
29. Zi F, Zhao DW and Zhang K. Image pre-processing algorithm based on lateral inhibition. In: *The eighth international conference on electronic measurement and instruments*, Xian, China, 2007, pp.121–122.

Appendix

Notation

A_i, A_{i+1}	inputs of the two units
D	dimensions of the search problem
e_p	output of unit without lateral inhibition
fitness()	fitness function
$I_0(m,n)$	original gray value of *pixel*(*m*,*n*)
k_{pj}	linear coefficients
$k_{i,i+1}$, $k_{i+1,i}$	linear coefficients of lateral inhibition
n	number of pigeons
$N_p(t)$	number of pigeons at tth iteration
$NC_{\max}$	maximum times of iteration
$NC1_{\max}$	iteration of map and compass operator
$NC2_{\max}$	iteration of landmark operator
$P(m,n)$	gray value of *pixel*(*m*,*n*) processed by lateral inhibition
rand	a rand number
Q	lateral inhibition matrix of 5×5 receptive field
r_{pj}^0	threshold value
r_p, r_j	outputs of two units
r_i, r_{i+1}	outputs of two units with lateral inhibition
$r_{i,i+1}^0$, $r_{i+1,i}^0$	threshold values of liner lateral inhibition
R	map and compass factor
$R_0(m,n)$	lateral inhibition competing coefficient of the *pixel*(*m*,*n*)
T	user-defined threshold of lateral inhibition
X_g	global best position
$X_c(t)$	center of pigeons at the tth iteration
X_i, V_i	position and the velocity of pigeon i
α_{00}	weight value of the center
α_1	surrounding weight value of the center
α_2	peripheral weight value
$\alpha_{i,j}$	lateral inhibition coefficient of *pixel*(*m*,*n*) to the central pixel
$\otimes$	convolution operation